SAND2020-2442C

Visualization and simulation of particle rearrangement and deformation during powder compaction

Marcia A. Cooper[1], Joel T. Clemmer[2], Michael S. Oliver[1], Dan S. Bolintineanu[2], Jeremy B. Lechman[2]

[1] Explosive Technologies
[2] Engineering Sciences
Sandia National Laboratories, PO Box 5800, Albuquerque, NM 87185

ABSTRACT
Two key mechanical processes exist in the formation of powder compacts. These include the complex kinematics of particle rearrangement as the powder is densified and particle deformation leading to mechanical failure and fragmentation. Experiments measuring the time varying forces across a densifying powder bed have been performed in powders of microcrystalline cellulose with mean particle sizes between 0.4 and 1.2 mm. In these experiments, diagnostics measured the applied and transmitted loads and the bulk powder density. Any insight into the particle behavior must be inferred from deviations in the smoothly increasing stress-density compaction relationship. By incorporating a window in the compaction die body, simultaneous images of particle rearrangement and fracture at the confining window are captured. The images are post-processed in MATLAB® to track individual particle motion during compression. Complimentary discrete element method (DEM) simulations are presented and compared to experiment. The comparison provides insight into applying DEM methods for simulating large or permanent particle deformation and suggests areas for future study.

Keywords: granular material, compression, fracture, discrete element method, imaging

INTRODUCTION

Granular materials are commonly processed for applications ranging from pharmaceuticals, to structural materials, to energy storage. Much of the literature data reports experimental compaction curves obtained at slow compression rates on materials where the particles have specific size, morphology, and surface characteristics. However, the compaction behavior of a granular material is strongly dependent on individual particle strength and characterization of the particle mechanics. Few models have incorporated representations of particle strength [1-3], while other particle characteristics of morphology and surface roughness are largely ignored. Computational methods including discrete element method (DEM) [4] and peridynamics [5] offer new capabilities in improved modeling treatments of granular materials in compression. Our efforts are aimed at developing a multi-scale, computational-experimental approach to create novel capabilities enabling process-structure-property-performance design and optimization of powder compacts.

Uniaxial and triaxial confined compression data of powders are common in the experimental literature. In compression, the processes of particle rearrangement, local elastic and plastic deformation, and fragmentation are all present to varying levels as determined by particle characteristics of strength, size, and shape. These levels often must be inferred from bulk measurements of boundary forces and bed volume. Previous experiments have visualized stress networks in optically accessible experiments [6]. The advancement of X-ray methods is affording new opportunities for particle visualizations in 3D [7-9]. However, current micro-computed tomography (micro-CT) technology has relatively large voxel sizes and long scan time durations that limit its usefulness to many particle systems of industrial interest.

Our research began with uniaxial confined compressions in a traditional cylindrical apparatus with microcrystalline cellulose (MCC) particles of different mean size [10]. We seek to avoid some of the immediate challenges of micro-CT imaging

during compression and instead simply apply optical access to our benchtop compression apparatus. This enables high-definition (HD) imaging of the particles during all compression regimes with adequate temporal resolution. Post-processing of the particle motion as viewed along the optically-accessible boundary is useful for correlating to particle simulations across the regimes of particle compression including fracture and crushing.

Granular systems are often simulated using the discrete element method. These models represent the system as a discrete collection of interacting particles. There are many varieties of DEMs and the fundamental particles can take on a wide range of shapes and sizes that interact via many different forces. Here, we present some initial DEM results using a model that represents the experimental compression apparatus dimensions and MCC particles. The DEM simulations were run using LAMMPS, a collection of parallel algorithms for the numerical integration of particle dynamics [4]. Model treatments for representing particle deformation and fracture are explored. Ultimately, our goal is to relate macroscale behavior (constitutive model) to particle characteristics as well as process to properties to structure.

GRANULAR MATERIALS

MCC particles consisted of Vivapur® MCC Spheres of type 350 and 1000 from JRS PHARMA (Weissenborn, Germany). The Vivapur® 350 (Batch No. 5135073146 X), and Vivapur® 1000 (Batch No. 5100070317 X) are referred to as V350 and V1000, respectively. Particle size distributions were measured with a Beckman Coulter LS 13 320 laser diffraction particle size analyzer with 50% of the particle size distribution equal to 0.473 ± 0.006 mm (V350) and 1.163 ± 0.128 mm (V1000). The particle shapes are roughly spherical and have internal porosity typically in form of a single void as shown in the images of Figure 1. Water content in the particles was measured by drying under vacuum at 105ºC for 24 hours and was nominally constant at 4.5%. Literature values for MCC report a value of the elastic modulus of 7.5 GPa [11].

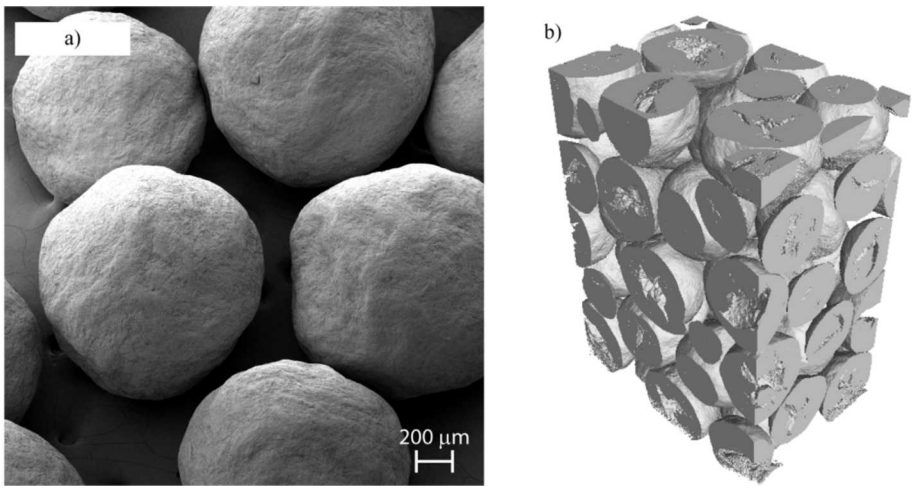

Figure 1. Scanning electron microscope (a) and micro-CT image (b) of V1000 particles showing nearly spherical particle shape and the existence of a single, large internal void.

COMPRESSION APPARATUS WITH OPTICAL ACCESS

The MCC particles are compressed uniaxially in a load-controlled manner by the apparatus of Figure 2. The apparatus consists of a pneumatic cylinder (Bimba Flat-I, Model FOS-1251.5-4GLV) to apply force to the top of a confined powder sample. A support structure vertically aligns the axis of the pneumatic cylinder to the axis of the confined sample. The sample is confined by the rectangular walls of the compression die body and confined axially by an upper and lower ram. Three walls of the compression die body are formed by a 304 stainless steel channel with height of 3.81 ± 0.02 cm, wall thickness of 1.91 ± 0.02 cm, and an inner channel that is 0.660 ± 0.02 cm square and machined for a loose slip fit to the square portion of the upper and lower rams. The fourth side of the confiner was 1.588 ± 0.02 cm thick borosilicate glass secured in place with a 0.953 ± 0.02 cm thick stainless-steel clamp which had a machined window that provided optical access to the test sample located in the inner channel. To cushion the interface between the confiner window and metal

surfaces, one layer of 68.6-μm-thick Kapton tape was used and included in the inner channel dimensions. The upper and lower rams are 304 stainless steel square bars machined to 0.645 ± 0.02 cm square to fit the inner channel of the confiner. The load cell end of each ram was turned to 0.643 ± 0.02 cm to mate to the load cell adapters. The lower ram is stationary while the position and force of upper ram is controlled by pressure within the pneumatic cylinder.

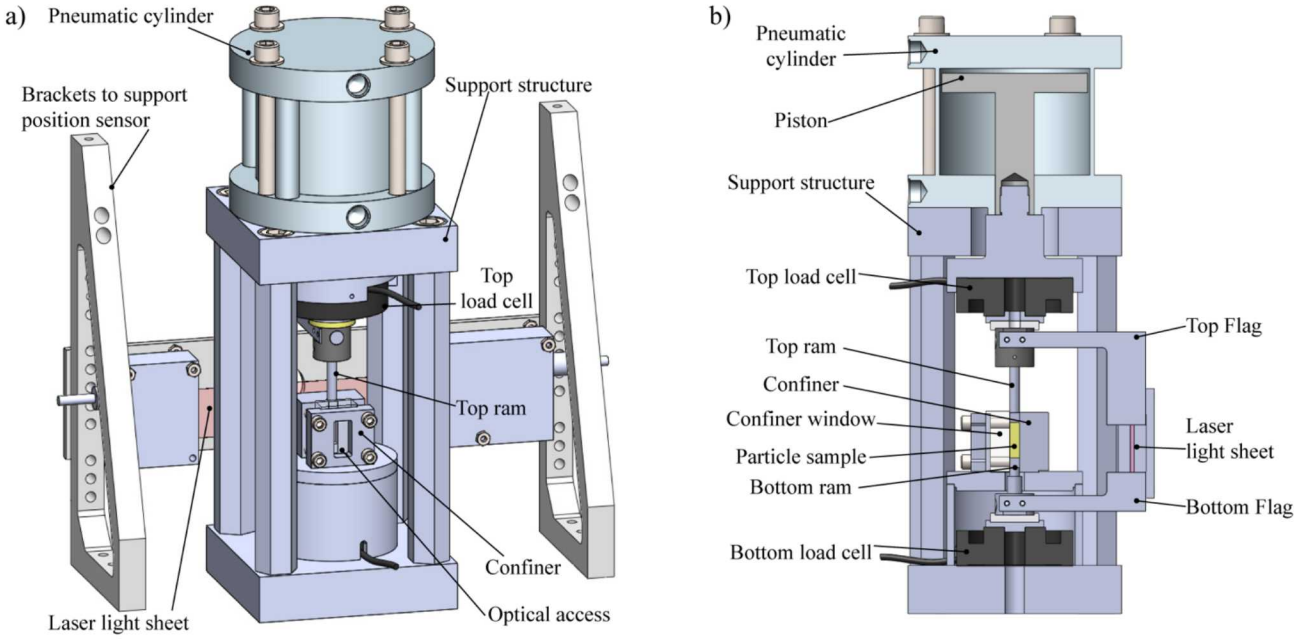

Figure 2. Illustration of the compression apparatus with optical access. (a) Isometric view. (b) Side view in cross section.

Each test began with a partially assembled compression apparatus by positioning the confiner/window body and lower ram onto the lower load cell (Transducer Techniques, Model THD-5K-T-OPT-HT). The sample material is weighed and poured into the confiner channel. For most tests, a carbide tipped hand held engraving tool (like McMaster Carr Part No. 1613T2) was used to vibrate the setup in order to settle the particles. The carbide tip was held against the plate the confiner rested on for a period of at least 30 seconds. Then, the upper ram is installed at the upper load cell (Transducer Techniques, Model THD-5K-T-OPT-HT) and plunger of the pneumatic piston such that it was elevated above the top surface of the particulate sample. The downward motion of the upper ram was initiated and the distance between the ram-mounted flags (Figure 2b) decreased as measured by the laser micrometer (Micro-Epsilon, Model 2500). Pressurization of the pneumatic piston is controlled with a LabView program and a voltage-controlled pressure regulator (Proportion-Air Model QB1SSFEE500) resulting in a constant rate of load applied by the upper ram. Force on the particulate sample increased at the preprogramed loading rate until the maximum load was achieved. The force was applied at a rate of 0.22 kN/min resulting in a varying displacement rate during compression nominally between 0.01 mm/s and 0.0001 mm/s. The maximum applied load was determined by the pneumatic cylinder's maximum pressure rating of 1.4 MPa and was connected to bottled air. The LabView program controlled the maximum applied force to 6.7 kN. During a test, the LabView program controlled the pneumatic cylinder pressurization and recorded the laser micrometer sensor and load cell data at a rate of 1 Hz. The maximum force was held for five minutes and then released.

Figure 3 plots the compression curve data from the compression apparatus with optical access (Figure 2) with the data from a cylindrical compression apparatus [10]. The data from the different compression experiments show good agreement in terms of applied stress and strain (Figure 3a). When plotted in terms of relative density and applied stress in a linear-log plot (Figure 3b), the new data from the optical compression apparatus begins at a lower tapped density. This is consistent with prior testing and is a trend with the aspect ratio (initial bed height/length scale of confiner cross section) of the powder bed [10]. The average aspect ratio for the data of Figure 3 is 2.1 (cylindrical) and 1.2 (optical).

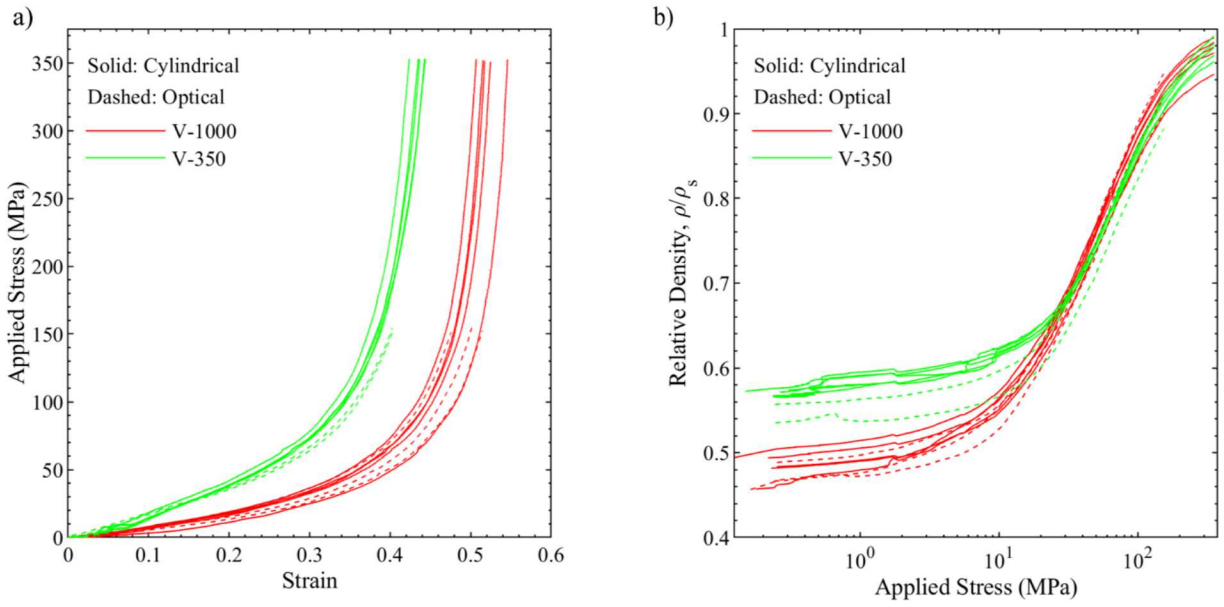

Figure 3. Data from compression apparatus with optical access (dashed lines) compared to prior data [10] from a cylindrical die body (solid lines) for V1000 and V350 particles. (a) Applied stress versus strain. (b) Relative density versus applied stress.

Video of each experiment was captured using a 2.1-megapixel HD CVI cube camera adapted to a K-Series long distance video microscope lens and recorded in HD format. Fiber-light illumination was directed into the side of the confiner window. Image size was 1920 x 1080 pixels and image magnification of nominally 152.5 px/mm. Frames extracted from a movie compressing V1000 particles appears in Figure 4. MCC particle fracture and crushing was observed earlier in the compression process at the boundary with the moving ram (at frame 101) and then throughout the particle bed in the later images (frame 151 and later) of the compression process. The fracture and crushing characteristics were consistent with observations in literature [12]. For the remainder of this work, only the optical compression data from the V1000 particles are presented and compared to simulations.

IMAGE PROCESSING FOR POWDER BED DEFORMATION

The HD images were processed in Matlab® following the typical initial process for marker-controlled segmentation. This process often precedes a watershed transformation to identify object boundaries. In these images, the slight transparency of the particles and relatively low contrast at the particle boundaries along with the increase in particle boundaries due to fracture and crushing prevented a direct application of watershed segmentation methods. Rather, the centroid of each particle was identified by finding the best marker location that was in the middle of each particle boundary in the gradient magnitude image. This was completed with a polar coordinate transformation and then a minimization of the radial distance from the found particle center and nearest boundaries in a region of interest about each marker. Several frames are extracted from the compression data with the found particle centers annotated by red dots (Figure 4). In general, the image processing found nearly all visible particle centers in successive frames such that quantitative evaluation of particle motion was possible.

The individual particle centers throughout the image sequence are annotated in Figure 5a illustrating how a particle moves along the optical window in time. The image colormap changes from cyan to magenta with increasing frame number. The particle centers are plotted in Figure 5b in terms of applied stress and axial strain. The applied stress (Figure 3) measured at the top ram at the time of the extracted frame is plotted on the y-axis. The x-axis strain corresponds to the strain experienced by each particle. Thus, for one compression experiment many stress-strain curves are extracted for the visible particles. Particle displacement is reported relative to the moving ram position and strain is calculated relative to the initial image frame at the start of the applied load.

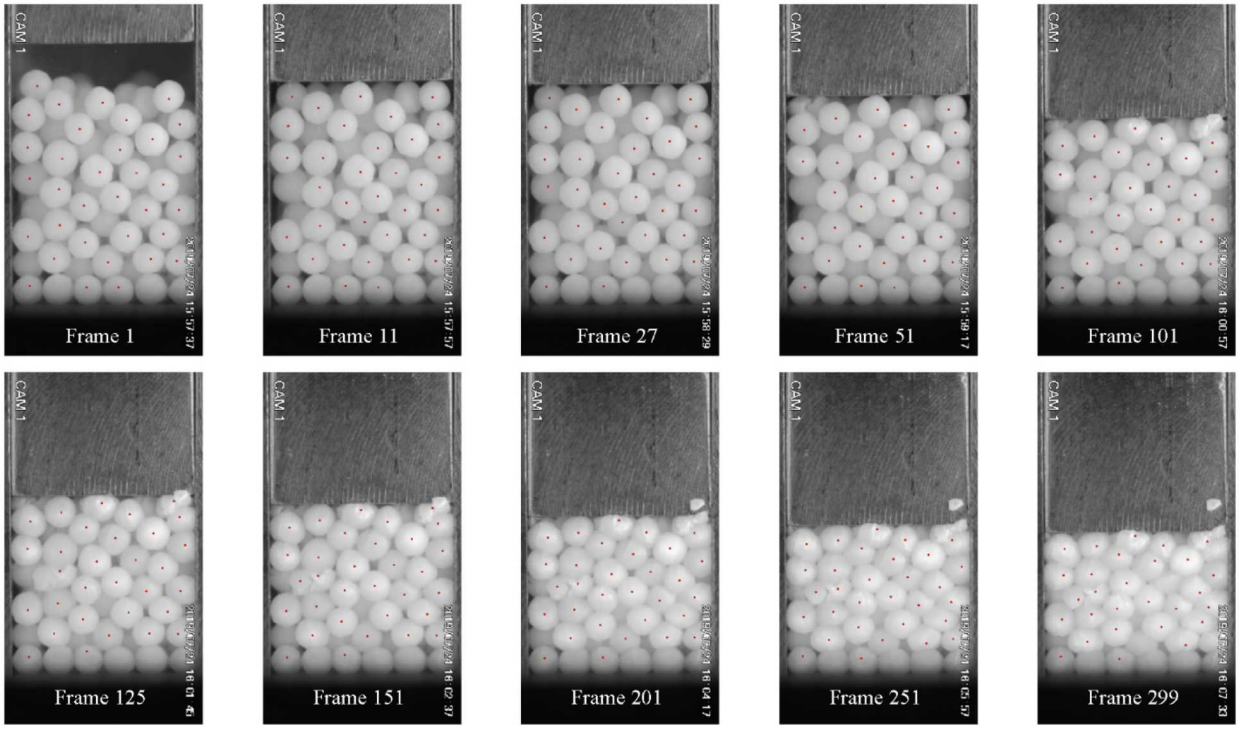

Figure 4. Frames extracted from high-definition movie collected during axial compression. The top ram moves downward in each image frame to compress the particles. The images are annotated with red dots representing the particle centers found through the image processing scheme.

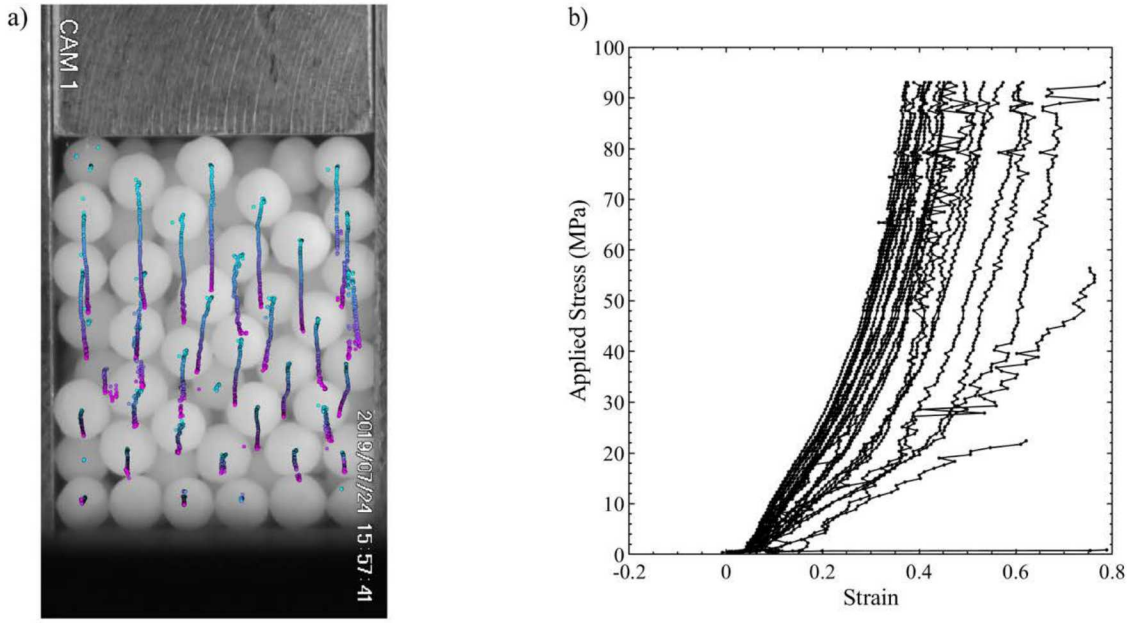

Figure 5. (a) Frame from image sequence at the start of compression annotated with particle position during compression. The colormap changes from cyan to magenta with increasing frame number. (b) Applied stress versus axial strain of particles.

SIMULATION BY DEM

One can subdivide DEMs into two classes, non-bonded and bonded models. In non-bonded models, each particle represents a single grain. This representation allows simulations to reach large scales representing millions of grains. Alternatively, each particle can represent a subdomain of an individual grain. A single grain is therefore made up of many particles which are

bonded together with a network of attractive forces that maintains cohesion. This representation allows the shape of grains to deform and allows for the possibility of fracture under a large enough applied force. We are developing both classes of DEMs and are exploring how initial simulation results compare to experimental measurements. These early results highlight qualitative changes in behavior and identify directions of future research.

Two DEMs are used to study the uniaxial loading of granular packings. The first DEM, referred to as the non-bonded model, represents each grain as a single particle. Each particle has translational as well as rotational degrees of freedom. Particles interact with Hertzian contact forces as well as tangential, rolling, and twisting forces. 125 particles were poured into a square box with frictional walls under gravity. Micro-CT images of the VP1000 samples found particles were nearly spherical suggesting this is a reasonable representation of the actual geometry. After particles settled, they were uniaxially compressed at a constant displacement rate. In Figure 6a, a system is rendered at a strain of 40%. Grains have significant overlap and one might expect to be beyond the limit of Hertzian contact.

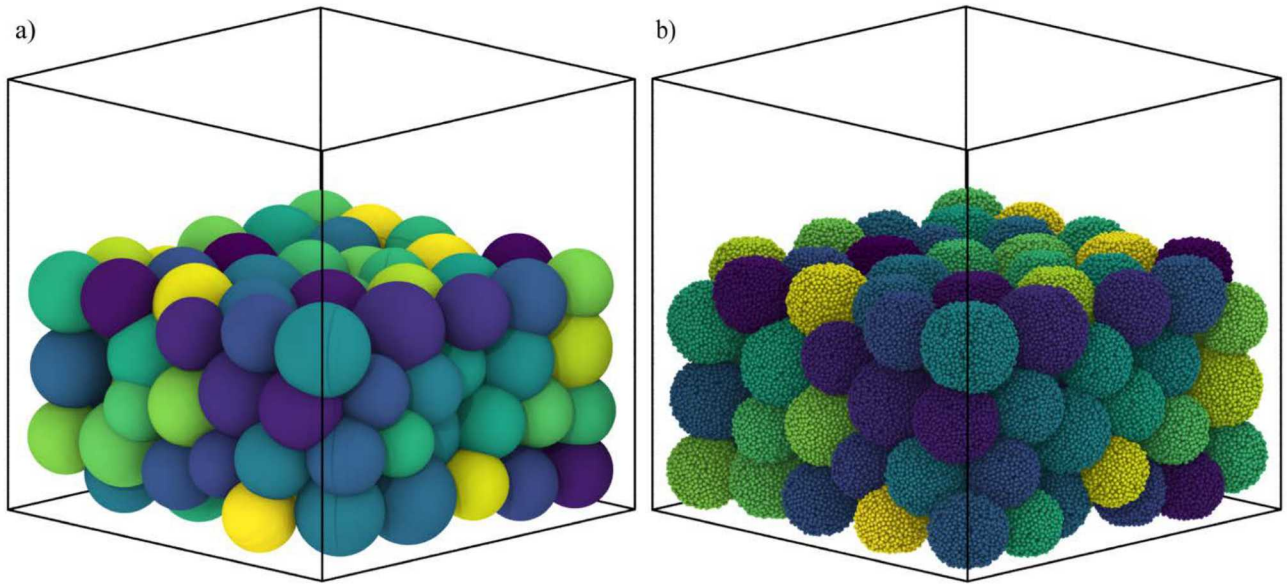

Figure 6. Rendered images of DEM simulations at 40% strain. In the non-bonded DEM (a) each grain consists of a single particle while in the bonded DEM (b) each grain consists of a few thousand particles. For the bonded DEM, λ_c is set to 1.5. Particles within each grain are colored uniformly. Note that the final configuration of grains differs.

The second DEM, the bonded model, represents each grain as a disordered collection of bonded point particles. While bonded, two particles interact with a piecewise potential. The potential has an equilibrium distance set to the initial distance r_0 between the particles to create a stress-free reference state. In compression, particles interact with a repulsive Lennard-Jones (LJ) interaction. In extension, an attractive interaction includes a harmonic term that is continuously smoothed to zero force at a distance of $\lambda_c r_0$ where λ_c represents a critical stretch. If a bond is stretched beyond this threshold, it is permanently broken. Non-bonded particles interact with a repulsive LJ interaction. Specifics of the model are discussed in Ref. [13]. Initially, particles within an individual grain are connected by bonds to provide cohesion. The same granular packing was used to initialize both the bonded and non-bonded DEM simulations. Systems were enclosed by frictionless, repulsive LJ walls and were uniaxially compressed. In Figure 6b, a sample system is rendered for $\lambda_c = 1.5$ at a strain of 40%. At this high value of the critical stretch, effectively no bonds break but the initially spherical grains undergo significant distortion. At smaller values of λ_c, one finds bonds breaking near the contacts. In Figure 4, one can see significant distortion of MCC grains as well as fracture at high strains suggesting that a bonded DEM is necessary to capture the experimental behavior at large pressures.

In Figure 7, normalized stress-strain curves are plotted for both the experimental system (Figure 3) and the two DEMs. The compressive stress is normalized by the elastic modulus of a grain. In the simulations, the strain is calculated using a reference geometry identified when the normalized compressive stress first exceeds 3×10^{-5} to avoid fluctuations at small

strains due to system preparation. In the nonbonded DEM, decreasing λ_c reduces the stiffness of the system and allows one to model a wide range of responses. It is suggestive that that the experimental results for the compression of MCC (Figure 3) lie between the limits of high and low λ_c. However, one cannot make any conclusions due to differences between the systems. For instance, the bonded DEM does not contain frictional walls nor do its grains contain internal porosity. We plan to explore these features in greater depth in the future.

Several of the bonded models show a discontinuity in the compression curves at low values of strain near 0.1 which corresponds to a large particle rearrangement event. We expect such discontinuities would be less observable for simulations with more particles producing a smoother compression curve.

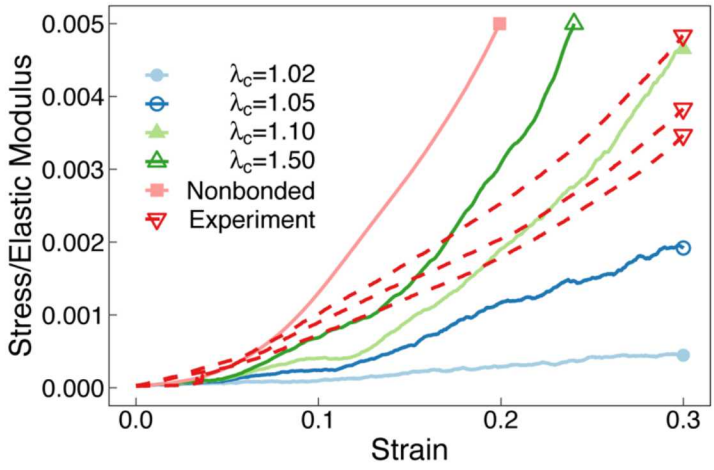

Figure 7. The compressive stress normalized by the elastic modulus is plotted as a function of strain from experimental and simulated systems.

CONCLUSION

We present a new experimental apparatus for compression of particles with the ability to watch the particle motion, deformation and ultimately fracture or crush. Through post-processing of the collected image sequence, the strain and stress for the particles is extracted and used for comparison to DEM simulations. For an initial effort, the comparison between the bonded DEM model with the bulk compression data appears promising. Future work on the advancement of DEM for the prediction of granular material compression will address friction and internal particle porosity.

ACKNOWLEDGEMENTS

This work is funded by Sandia's Laboratory Directed Research and Development program. Sandia National Laboratories is a multimission laboratory managed and operated by National Technology & Engineering Solutions of Sandia, LLC, a wholly owned subsidiary of Honeywell International Inc., for the U.S. Department of Energy's National Nuclear Security Administration under contract DE-NA0003525. This paper describes objective technical results and analysis. Any subjective views or opinions that might be expressed in the paper do not necessarily represent the views of the U.S. Department of Energy or the United States Government.

REFERENCES

[1] Adams, M.J. and McKeown, R. "Micromechanical analyses of the pressure-volume relationship for powders under confined uniaxial compression". *Powder Technology*, *88*(2), pp. 155-163 (1996).

[2] Krairi, A., Matouš, K. and Salvadori, A. "A poro-viscoplastic constitutive model for cold compacted powders at finite strains". *International Journal of Solids and Structures*, *135*, pp. 289-300 (2018).

[3] Kenkre, V.M., Endicott, M.R., Glass, S.J. and Hurd, A.J. “A theoretical model for compaction of granular materials”. *Journal of the American Ceramic Society*, 79(12), pp. 3045-3054 (1996).

[4] Plimpton, S. “Fast Parallel Algorithms for Short-Range Molecular Dynamics”, *Journal of Computational Physics*, 117, pp. 1-19 (1995).

[5] Silling, S. A., and Ebrahim A. “A meshfree method based on the peridynamic model of solid mechanics”. *Computers & Structures,* 83(17-18), pp. 1526-1535 (2005).

[6] Hurley, R., Marteau, E., Ravichandran, G. and Andrade, J.E. “Extracting inter-particle forces in opaque granular materials: beyond photoelasticity”. *Journal of the Mechanics and Physics of Solids*, *63*, pp.154-166 (2014).

[7] Jin H. et al. Multiscale XCT Scans to Study Damage Mechanism in Syntactic Foam. In: Lin MT. et al. (eds) Advancements in Optical Methods & Digital Image Correlation in Experimental Mechanics, Volume 3. Conference Proceedings of the Society for Experimental Mechanics Series. (2020).

[8] Hurley, R.C., Lind, J., Pagan, D.C., Akin, M.C. and Herbold, E.B. “In situ grain fracture mechanics during uniaxial compaction of granular solids”, *Journal of the Mechanics and Physics of Solids*, 112, pp. 273-290 (2018).

[9] Erikson, W.W., Cooper, M.A., Guo, S., Roberts, S.A. and Bolintineanu, D.S. “CT scan characterization of thermally damaged energetic materials”. In: Proceedings of the 15th International Detonation Symposium. Cambridge, MD. (2018).

[10] Cooper, M. A., Oliver, M.S., Bufford, D.C., White, B.C., and Lechman, J. “Compression Behavior of Microcrystalline Cellulose Spheres: Single Particle Compression and Confined Bulk Compression Across Regimes”. *Powder Technology*, Submitted (2020).

[11] Jonsson, H. and Frenning, G. “Investigations of single microcrystalline cellulose-based granules subjected to confined triaxial compression,” *Powder Technology,* 289, pp. 79-87 (2016).

[12] Jonsson, H., Öhman-Mägi, C., Alderborn, G., Isaksson, P. and Frenning, G. “Crack nucleation and propagation in microcrystalline-cellulose based granules subject to uniaxial and triaxial load”. *International Journal of Pharmaceutics*, 559 pp. 130-137 (2019).

[13] Clemmer, J.T. and Robbins, M.O. “Critical Scaling of Fragment Sizes in Comminution of Brittle Solids”. Manuscript in Preparation (2020).